PAPER

Probing hole-doping of the weak antiferromagnet TiAu with first principles methods

IOP Publishing Journal of Physics: Condensed Matter
J. Phys.: Condens. Matter **31** (2019) 074005 (10pp) https://doi.org/10.1088/1361-648X/aaf689

Probing hole-doping of the weak antiferromagnet TiAu with first principles methods

Milena Mathew, Wen Fong Goh and Warren E Pickett

Department of Physics, University of California Davis, Davis, CA 95616, United States of America

E-mail: wepickett@ucdavis.edu

Received 20 September 2018, revised 28 November 2018
Accepted for publication 5 December 2018
Published 7 January 2019

Abstract

We investigate hole-doping by Sc substitution for Ti in the weak antiferromagnet (wAFM) system $Ti_{1-x}Sc_xAu$. Behavior reported so far fits a weak *itinerant* AFM picture, and experimentally leads to a quantum critical point at $x_c = \frac{1}{8}$. Here we study supercells with several rational fractions x of Ti replaced by Sc. We find, unexpectedly, definite local moment-like behavior, e.g. magnetic moments of the Ti atom comparable to or even larger than in the bulk persist even into the Ti-poor regime of this alloy system. Itinerant signatures persist, however, as the Ti 3*d* projected density of states displays van Hove singularity peaks near the Fermi level in most cases, revealing a striking similarity to nonmagnetic bulk TiAu. The current picture of this system, midway between itinerant and local moment, will be provided and discussed in light of experimental observations.

Keywords: itinerant magnetism, quantum critical point, hole doping, interacting local moments, density functional theory

(Some figures may appear in colour only in the online journal)

1. Introduction

Weak antiferromagnetism (wAFM) is a rare occurrence in crystalline condensed matter, in fact, several weak magnets originally identified as wAFMs have been found to be ferromagnetic (sample dependence can be strong) [1–3]. A recent topical review has been provided by Santiago *et al* [4]. Weak atomic moments arise within spin density waves (SDWs), where small moments can be interspersed with near-zero moment atoms, although these are usually not included in the class of wAFMs. SDWs are connected with a wavelength, i.e. *a wavevector* $\vec{Q}$ with the mechanism tied to Fermi surface calipers. The example that we consider in detail here is the wAFM TiAu reported by Svanidze *et al* [5], which presents several questions yet to be resolved.

First, elemental Ti is a non-magnetic metal, in column IVB of the periodic table in which the heavier members are never magnetic except for the weak ferromagnet $ZrZn_2$ [6, 7]. Ti is almost never magnetic in binary metallic compounds, with weak ferromagnetic $TiBe_2$ [9, 10] being the other exception besides TiAu. In each of these three weak magnets, large and narrow peaks occur accidentally at the Fermi level, arising from a pair of nearby van Hove singularities (vHs) at which the large Fermi surfaces are changing topology. The large value of the electronic density of states $N(E_F)$ at the Fermi energy E_F promotes the Stoner instability [8], driving two of them ferromagnetic.

Stoichiometric TiAu was found [5] to undergo AFM order at $T_N = 36$ K, with a Curie–Weiss moment of $m_{CW} = 0.8\ \mu_B$ and a small ordered moment of $0.15\ \mu_B$. Neither is characteristic of a local moment, leaving the designation as an itinerant wAFM such as has been studied by Moriya and collaborators [11, 12] and reviewed by von Löhneysen *et al* [13]. The nonmagnetic band structure was found to display a narrow and sharp peak in the electronic density of states (DOS) [5, 14, 15], with implications that will be reviewed at the beginning of section 3.

TiAu can be driven to the quantum critical point $T_N \to 0$ by replacing 12%–13% of Ti with Sc; we will adopt the critical concentration value $x_{cr} = \frac{1}{8}$. Besides depleting the magnetic

Ti sublattice, this alloying does several things. (1) It lowers the Fermi level by $\frac{1}{8}$ electron/f.u., thus moving the Fermi level E_F well away from the undoped, nonmagnetic vHs peak, as shown below. Such a pronounced peak is a common cause of magnetic (Stoner) instability. Even a small amount of doping might be expected to reduce or remove the already (presumably) weak tendency of the Ti atom to polarize. (2) Substitution disrupts the exchange coupling between Ti atoms, which includes in addition to the local coupling processes the longer range RKKY interaction through the (mostly Au $s-p$) electron gas, by altering the Fermi surfaces. (3) Substitution introduces disorder, causing broadening of the Fermi surface, thereby reducing the range of interatomic RKKY coupling. (4) In the cases where Ti atoms retain magnetism, Sc may lead to widely varying and frustrating Ti–Ti exchange interactions.

Svanidze *et al* [16] characterized this alloy system to and beyond the quantum critical point (QCP), finding non-Fermi liquid (nFL) behavior near x_{cr}. The resistivity approaches linear in temperature T at the QCP, while the residual resistivity increased only by a factor of four, the latter indicating minor disorder effect. The linear specific heat coefficient $\gamma(x)$ becomes logarithmically divergent as $x \to x_{cr}$, presumably from enhanced spin fluctuations. The physical properties near the QCP were judged to be more characteristic of two dimensional (2D) spin fluctuations and 2D nFL than the 3D behavior, although the crystal structure and metallic conduction away from the QCP are representative of a 3D metal.

To broaden the picture, electron doping with vanadium $Ti_{1-y}V_yAu$ has recently been reported by Huang *et al* [17] up to the solubility limit $y_s = 0.15$, where $T_N = 8$ K is still well short of the QCP in this direction. Nonetheless, signatures of nFL behavior were observed in transport and heat capacity. Based on x-ray diffraction peak widths and residual resistivity, V substitution leads to larger disorder effects than does Sc substitution. As for the hole-doped case, the AFM peak in magnetization $M(T)$ at the ordering transition becomes rounded rapidly upon doping.

Differences between the behavior of metallic wAFMs versus wFMs near their QCPs has been a topic of theoretical study. One focus has been relevance of 'rare regions', that is, droplets of randomly placed, locally ordered clusters in the paramagnetic phase that interact at long range by RKKY interactions. In wFMs, these interactions tend to support long range order. In wAFMs, on the other hand, a cluster glass phase will appear between the ordered and paramagnetic phases, caused by cluster-derived dissipative mechanism beyond the dissipative effects of the gapless metallic background [18–20]. Doped TiAu provides a platform to begin to evaluate the applicability of these ideas.

With these issues in mind, we have carried out first principles calculations on ordered supercells of $Ti_{1-x}Sc_xAu$. We find that they provide insight into the microscopic character of the alloy system, with local moment characteristics indicating that disorder may have a substantial impact in driving $Ti_{1-x}Sc_xAu$ to the quantum critical point. Along the way we obtain information about the electronic state of the system beyond the QCP.

The organization of the paper is as follows. Section 2 gives a description of the methods of calculation that are used, the crystal structure, and an introduction to the supercells that are used. Section 3 provides a summary of previous electronic and magnetic structure results. In section 4 the results of the supercell calculations are provided is some detail. Then section 5 provides a discussion and summary of results.

2. Methods and structure

2.1. Methods

Calculations using the local spin-density approximation implemented in FPLO 14.00 [21], a full potential local-orbital minimum-basis code, were used to determine the effects of substituting a fraction of Ti sites with Sc atoms using supercells. The local density approximation (LDA) [22] exchange-correlation functional was used, because it was found previously [15] that the Ti magnetic moments were larger using the generalized gradient approximation [23] (GGA) than with LDA, which itself predicts moments larger than observed. This incorrect tendency of GGA to overestimate magnetism has been documented in a number of materials [24–27]. The calculations were spin polarized, using antiferromagnetic starting configurations representative of AFM TiAu. Calculations were done self-consistently with a convergence tolerance of 10^{-6}. A $12 \times 12 \times 12$ k-mesh was used in the AFM cell, with comparable mesh spacings for the supercells. Denser meshes, namely $24 \times 24 \times 24$, were used for some of the DOS plots.

2.2. Structure and supercells

TiAu crystallizes in the *Pmma* space group (#51) with two formula units in the orthorhombic primitive cell, with $a = 4.62$ Å, $b = 2.92$ Å, $c = 4.90$ Å. The atomic positions are Ti $2e$ at (0.25,0.0,0.3110), Au $2f$ at (0.25,0.50,0.818). AFM order, see figure 1, arises along the Ti linear chains along the b axis, where the Ti–Ti separation is $d_1 = b = 2.92$ Å. This bond length is only slightly shorter than that of the zigzag chain along the a direction, $d_2 = 2.96$ Å. Note that these separations are extremely close to that of hcp Ti, 2.95 Å. The Stoner enhancement factor of elemental Ti [28] is 1.36, well away from a ferromagnetic instability. The smallest distance between a Ti and another Ti in the next cell in the c direction is much longer, $d_3 = 3.82$ Å. Thus magnetic interactions can be expected to be dominated by two direct Ti–Ti exchange constants corresponding to a corrugated $a-b$ plane of atoms (see figure 1), supplemented by three dimensional RKKY interactions to more distant neighbors mediated by the electron gas.

Two unit cells are needed for the observed AFM ordering in TiAu, specifically, doubling along the b axis: Ti_4Au_4. To allow some remnant of this AFM order to emerge as doping proceeds, the supercell should contain multiples of this AFM cell: $Ti_{4n}Au_{4n}$. If p Ti atoms are replaced by Sc, the Sc concentration is $x = \frac{p}{4n}$.

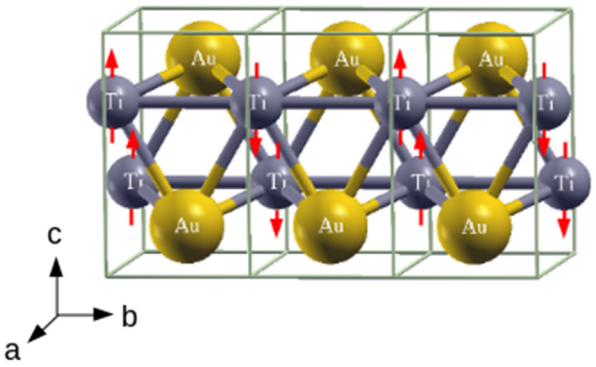

Figure 1. Crystal and magnetic structure of antiferromagnetic TiAu, showing aligned layers alternating in spin direction along the *b* axis. This underlying AFM order is used to guide that in the hole-doped cells.

3. Previous results; nonmagnetic reference

3.1. Summary of earlier theoretical results

Two of the current authors have presented results for stoichiometric TiAu. The first paper addressed the microscopic mechanism leading to wAFM in TiAu. The ordering wavevector $\vec{Q}^{\rm AFM} = (0, \pi/b, 0)$ is not where the strongest nesting occurs [14]. However, $\vec{Q}^{\rm AFM}$ is close to the wavevector $\vec{Q}^{\rm vHs}$ separating van Hove singularities. Examining the Kohn–Sham–Lindhard susceptibility $\chi_o(\vec{Q}^{\rm vHs} + \vec{q}, \omega)$, it was found that in the small $\vec{Q}$, small ω, regime, the susceptibility has $\vec{q}$ and ω dependences identical to that arises from ferromagnetic fluctuations, and competes on equal ground with the Stoner instability (which involves a single vHs). AFM fluctuations win, and commensuration effects, namely strain, drives the ordering vector to the observed commensurate one. This viewpoint provides a reason why TiAu is a wAFM while $ZrZn_2$ and $TiBe_2$ are weak ferromagnets.

Further work [15] looked more closely at the main vHs (with surprisingly heavy masses $m_{\rm th} = |m_x m_y m_z|^{1/3} = 7.7 m_e$ for the main vHs), studied Fermi surface nesting, and investigated the competition between FM and AFM tendencies. A central finding was, compared to the experimental ordered moment of 0.15 $\mu_{\rm B}$, the calculated Ti moment is 0.84 $\mu_{\rm B}$ in GGA, and 0.40 $\mu_{\rm B}$ in LDA. Such overestimates of moments are not uncommon, and can be ascribed to neglect of magnetic fluctuations in a DFT calculation. Using the approach of Ortenzi *et al* [26] to account for fluctuations, a reduction of the exchange potential by 45% would reduce the LDA moment to the experimental value. Reducing the GGA value to experiment would require an even larger renormalization. For this reason, it was concluded that using LDA for TiAu is more reasonable than using GGA.

The magnetic moment for FM alignment and varying Sc concentration was studied in the virtual crystal approximation [15] (VCA) using the fixed spin moment method, for both hole and electron doping. Using LDA, the critical concentration where the moment vanished for hole doping was overestimated by a factor of two, $x = 0.26$ versus the experimental $x_c = \frac{1}{8}$. Using the Ortenzi renormalization, the critical value was too small, $x = 0.05$. We have now carried out the LDA VCA study for hole doping with AFM order, and find the same critical point $x = 0.25$. This similarity of the AFM and FM moments and their trend with doping seems peculiar from the itinerant magnetism viewpoint, since the electronic structures are substantially different for the two alignments. We note that these overestimate of magnetic tendencies underlines the uncertainties in absolute numbers that one must deal with when applying spin density functional theory to the weak magnetism in TiAu, but trends in the magnetic behavior are predicted more reliably.

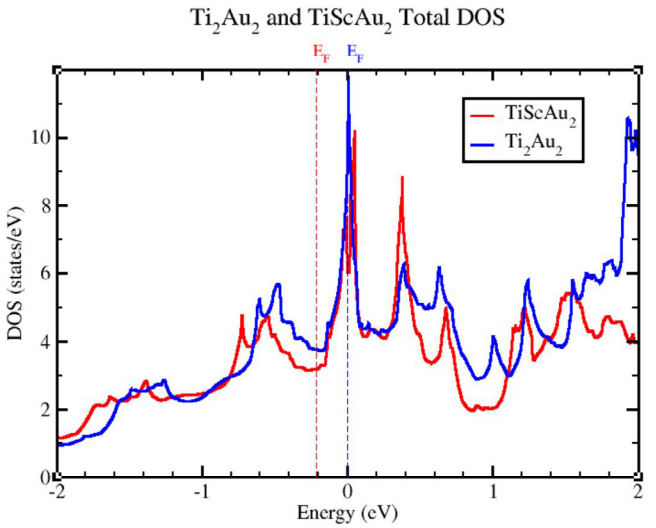

Figure 2. Comparison of nonmagnetic DOS of Ti_2Au_2 and $TiScAu_2$. The energy zero is aligned for equal band filling at the Fermi level of TiAu $\equiv Ti_2Au_2$.

3.2. Nonmagnetic $TiScAu_2$ versus Ti_2Au_2

For orientation, we first consider without consideration of magnetism what replacement of Ti by Sc does to the electronic structure. The DOS curves of Ti_2Au_2 and $TiScAu_2$ are compared in figure 2. These curves have been aligned at the same band filling, the Fermi level of Ti_2Au_2 at 30 electrons/f.u. The first observation is that this 50% ordered substitution lowers $E_{\rm F}$ by 0.2 eV, from the vHs peak of TiAu to a valley for $TiScAu_2$. This reduction should remove the Stoner instability toward ferromagnetism, and indeed a ferromagnetic ground state is not predicted. The nearly identical shape of the two DOS curves between the two Fermi levels indicates that, without magnetism, an itinerant rigid band behavior is not obtained.

The Ti $\rightarrow$ Sc substitution introduces a fine structure splitting of the vHs peak, hardly visible in figure 2. The 0.1 eV splitting is however moderate, and the DOS remains high at that band filling. However, that region of the DOS becomes irrelevant as Sc is added, lowering the Fermi level. The peaks in the -0.7 to -0.5 eV region remain but are lowered by Sc substitution, suggesting *d* band broadening. The peaks at 0.4 eV and 0.6 eV remain undisplaced, while the next two peaks are displaced by 0.2 eV to 0.4 eV higher energy, again indicating broadening of

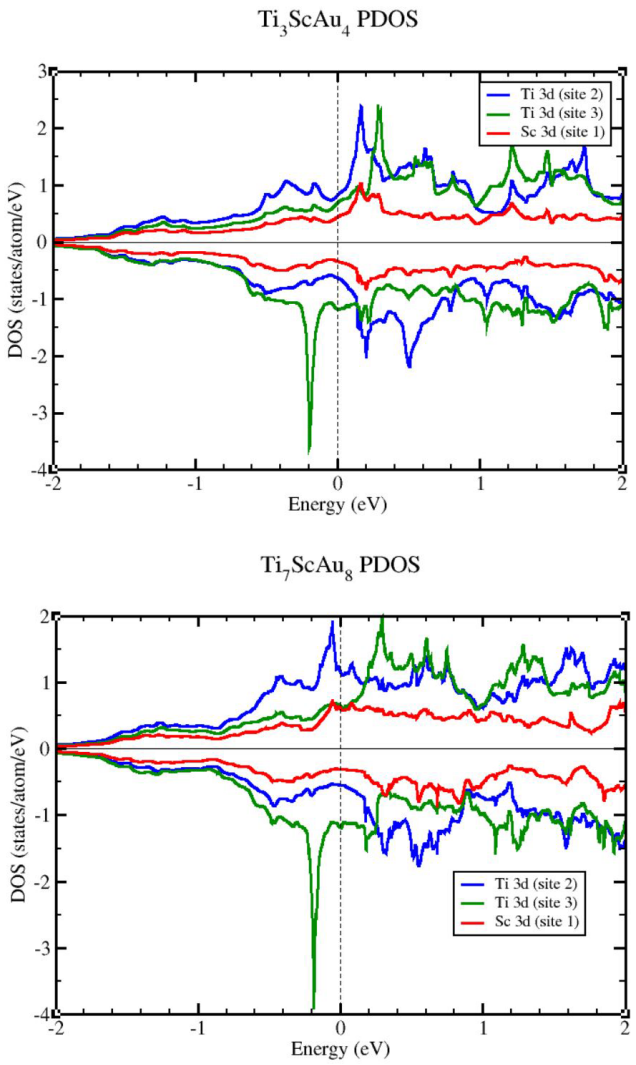

Figure 3. Comparison of 3*d* PDOS for two cells with a single Sc atom: top, for the 1/4 cell, and bottom, the 1/8 cell. The narrow peak, plotted downward here, at −0.2 eV is remarkable similar in these two single-Sc cells.

the *d* bands. The full $TiScAu_2$ PDOS mimics the shape of that of Ti_2Au_2 throughout, consistent with fully itinerant Bloch states that naturally have more density on Ti than on Sc. The disappearance of magnetism can be understood from the point of view of the Stoner mechanism requiring a large $N(E_F)$. All of this behavior seems consistent with itinerant magnetism.

4. Supercell studies of hole-doping

In this section we provide, using supercells and thereby including local real-space interaction effects, several examples for a variety of hole doping levels. Emphasis is on the magnetic moments in relation to the geometry, and to energetic positions in the spectrum from various sites. We note first that Sc is never found to display a magnetic moment, since the small calculated values (less than 0.1 μ_B) can be ascribed to parasitic polarization from neighboring Ti moments. Ti atoms, on the other hand, persist in presenting magnetic moments of the order of 0.5 ± 0.1 μ_B well beyond the observed critical concentration $x_{cr} = \frac{1}{8}$. Occasionally a magnetically dead Ti site appears, then for large x all magnetism disappears.

4.1. $n = 1$ cell, $x = j/4$

For this basic cell, not pictured, think n terms of the left half of the sites shown in figure 4. For Ti_3ScAu_4 any choice of site for Sc is equivalent to any other. The supercell contains one Ti–Ti chain and one Ti–Sc chain along the $\hat{b}$ axis. The calculated ground state has aligned Ti spins across the chains (along a), with moments of moments of -0.63 μ_B and -0.41 μ_B (the magnitude of the bulk AFM moment is 0.45 μ_B). The other Ti site, between two Sc atoms along the $\pm a$ directions, is magnetically dead (a $+0.08$ μ_B parasitic moment) and there is negligible moment on Sc ($+0.05$ μ_B). Thus this level of (ordered) doping destroys the AFM order of the $\hat{b}$ axis directed chain.

From the PDOS in the top panel of figure 3, the dead Ti site (labeled site 2) can be seen to be unpolarized, as is Sc. The Ti with the largest moment (site 3) is strongly polarized. In the 3*d* PDOS, E_F lies in DOS valleys in both spin directions, a condition that often stabilizes a magnetic state. The majority (down) spin direction has a high and sharp vHs peak that lies 0.2 eV below E_F associated with the magnetic Ti sites. The minority spin has a corresponding peak at $+0.3$ eV, seemingly a Stoner splitting of 0.5 eV on Ti(3). These PDOS peaks arise from van Hove singularities and will be seen to be persistent for the larger cells to follow.

4.2. $n = 2$ cell, $x = j/8$

Since we are most interested in tendencies toward AFM ordering along the b axis directed chain, the primitive cell is doubled along the b axis. The ordering of Ti (Sc) sites is given in the caption of figure 4, and is identical in all the structure figures. Since Au site will never be discussed, the relevant Ti (Sc) sites are:

first row: 1, 2, 9, 10;
third row: 3, 4, 11,12.

Recall that the AFM structure of TiAu consists of rather well separated layers perpendicular to $\hat{c}$, with antialigned Ti spins along the $\hat{b}$ axis, in phase along the $\hat{a}$ axis. Doubling the AFM cell could be done along any of the three axes, however the small Ti–Ti distances within the $\hat{a} - \hat{b}$ plane suggests doubling in the layer. For this $n = 2$ case we have chosen supercells doubled along the a axis.

4.2.1. $x = 1/8$ *case,* Ti_7ScAu_8. The supercell structure and magnetic order is pictured in figure 4. The ground state magnetic arrangement is basically that of the host Ti AFM order but with a magnetically dead Sc site. However, the Ti moments range in magnitude from 0.34 μ_B to 0.69 μ_B, this maximum value being substantially larger than the 0.45 μ_B bulk value. All moments are listed in table 1. In the bottom panel of figure 3 a large peak for a down spin Ti(3), comparable sharpness and height to the peak of nonmagnetic TiAu at its Fermi level [15], lies 0.2 eV below E_F, exactly where a virtually identical

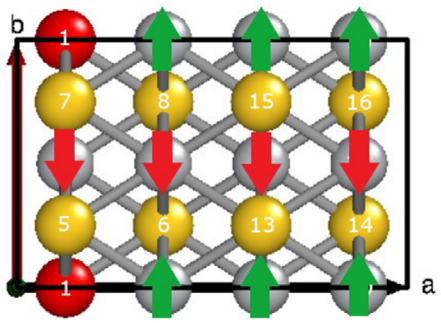

Figure 4. View along the c axis of the Ti_7ScAu_8 cell, providing the Ti site labels. Ti: gray; Sc: red; Au: yellow. The site numbers are: first row, 1, 2, 9, 10; second row, 7, 8, 15, 16; third row, 3, 4, 11,12; fourth row, 5, 6, 13, 14. The gold sites (second and fourth rows) are invariant and nonmagnetic, and will never be cited in the text.

Table 1. Moments (μ_B) for the $x = 1/8$ supercell Ti_7ScAu_8. The magnetic order is that of bulk TiAu with one dead (Sc) site.

Atom	Site	Moment
Sc	1	−0.03
Ti	2	0.34
Ti	3	−0.69
Ti	4	−0.43
Ti	9	0.49
Ti	10	0.33
Ti	11	−0.41
Ti	12	−0.43

peak occurs in the $x = 1/4$ in the upper panel. This peak is associated with Ti(3), with the large moment $-0.69\ \mu_B$. Note that Ti(3) lies between Sc sites along the zig-zag chain in the *hatb* direction. The PDOS peaks in the opposite spin direction are separated by 0.3 eV across the Fermi level.

This occurrence of strong PDOS peaks associated with specific Ti sites is more characteristic of local moment behavior than of itinerant behavior, where many or all Ti sites would contribute rather uniformly, thereby contributing to each DOS peak. Likewise, a Ti moment 50% larger than the bulk value suggest local moment character. This tendency toward single Ti site DOS peaks and local magnetism extends to the supercells discussed below.

4.2.2. $x = 2/8$ case: $Ti_6Sc_2Au_8$. The number of distinct configurations increases with supercell size and as the number of Sc sites increases. One configuration that can be avoided is the Ti_3ScAu_4 cell discussed above, simply doubled. The three configurations we have studied are shown in figure 5. C2 (configuration 2) has a single Ti chain replaced by Sc. The other two configurations have the second Sc atom one (C1), or respectively two (C3), chains distant.

In C2 all sites along the Sc chain are dead. The order can be described as aligned triplets of Ti atoms along the $\hat{a}$ direction, antialigned with the parallel chain in the unit cell. Put another way, it is TiAu with every fourth $\hat{b}$-axis directed chain removed. In both C1 and C3 the $\hat{b}$ axis chain is interrupted by Sc. However, both are still characterized by FM aligned triplets along a directed rows, the other chain has identical but

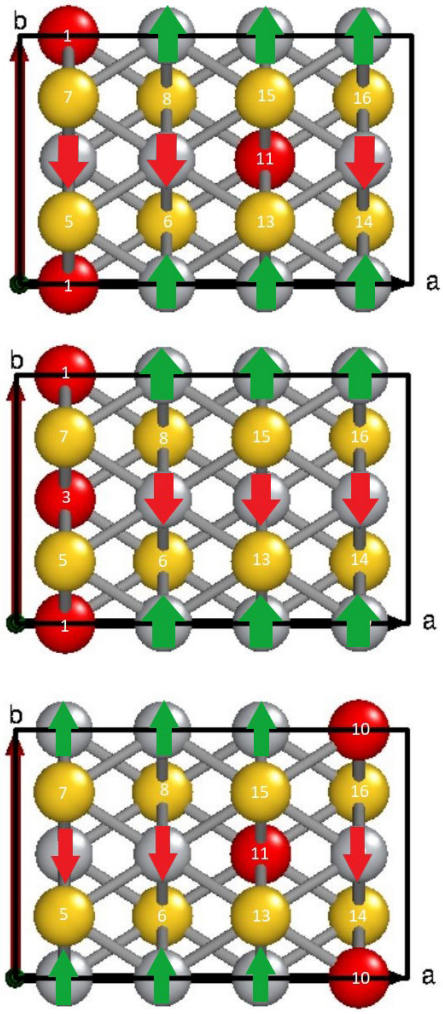

Figure 5. View along the c axis of configurations C1, C2, C3 (top to bottom, respectively) of $Ti_6Sc_2Au_8$. Ti: gray; Sc: red; Au: yellow:1. Configuration 2 replaces all Ti with Sc along a single b-directed chain.

Table 2. Moments (μ_B) of the $Ti_6Sc_2Au_8$ for the three configurations C1, C2, C3. Site labels are in the first column, and Sc moments are in brackets.

Site	C1 moment	C2 moment	C3 moment
1	[−0.05]	[−0.04]	0.28
2	0.31	0.30	0.46
3	−0.72	[−0.04]	−0.46
4	−0.31	−0.30	−0.28
9	0.72	0.46	0.55
10	0.31	0.30	[−0.03]
11	[0.05]	−0.46	[0.03]
12	−0.31	−0.30	−0.55

oppositely directed chains, out of phase along the a axis. All three are strictly AFM (but with internal structure) magnetic order. The moments, ranging from 0.30 to 0.46 μ_B in magnitude for C2 and in the range 0.28–0.72 μ_B for C1 and C3, are provided in table 2.

The corresponding $3d$ PDOS for selected sites are provided in figure 6. The PDOS show overall similarity (choice

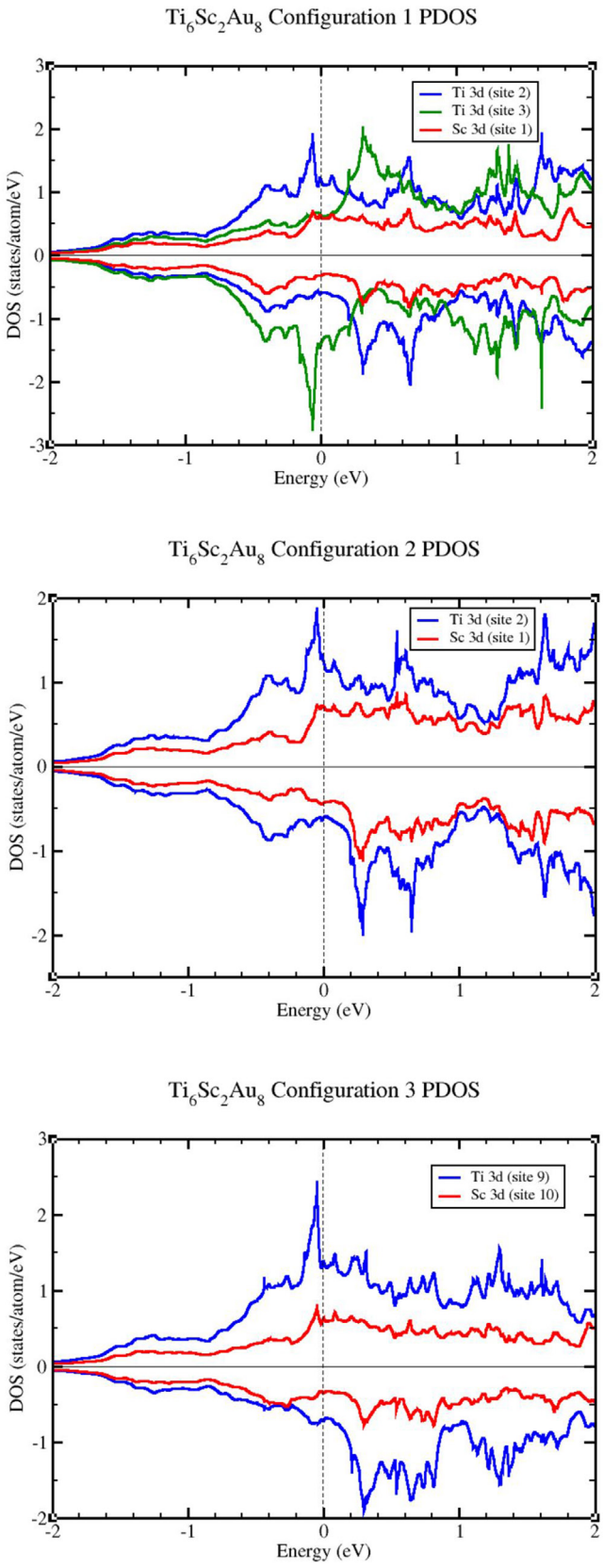

Figure 6. Comparison of selected 3*d* projected DOS for $Ti_6Sc_2Au_8$ configurations, with C1, C2, C3 from top to bottom.

of up versus down spin in each plot is arbitrary). There is a majority PDOS peak for the Ti atom(s) lying around −0.1 eV in all cases. Above E_F, the minority PDOS is larger in the 0.2

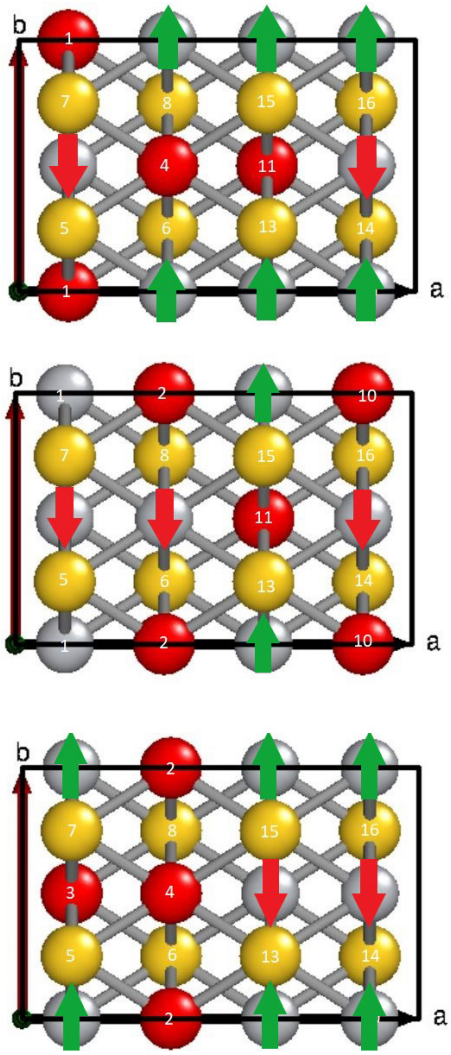

Figure 7. View along the *c* axis of configurations 1, 2, 3 (top to bottom, respectively) of $Ti_5Sc_3Au_8$. Ti: gray; Sc: red; Au: yellow:1.

eV–0.8 eV range. The Sc 3*d* PDOS shows much less structure than that of Ti and does not participate in the sharp, narrow peaks. These results again tend to support some effective local moment tendencies of the Ti atoms.

4.2.3. $x = 3/8$ *case:* $Ti_5Sc_3Au_8$. For this concentration, well beyond the experimental critical concentration for long range order, we have again looked at three configurations, specified in figure 7, the corresponding PDOS shown in figure 8, and moments in table 3. C1 consists of three of the four $\hat{b}$-axis directed chains being interrupted by Sc, with one out of phase with the other two. Considering the $\hat{a}$-axis, one chain has a triple of Ti before a Sc atom is encountered, the other has only a double of Ti atoms. For C2, three of the $\hat{b}$-axis chains are disrupted by Sc, one is not. For C3, two $\hat{b}$-axis chains are uninterrupted, while one chain has Ti replaced entirely by Sc.

C1 has a magnetically aligned triple of strong Ti moments along the $\hat{a}$-axis, the other has a pair of Ti atoms. This latter pair has rather weak (0.21–0.26 μ_B) but aligned moments. The triples have aligned strong moments. C2 has a weak moment (0.13 μ_B) Ti(9) atom, being surrounded entirely by Sc atoms in the

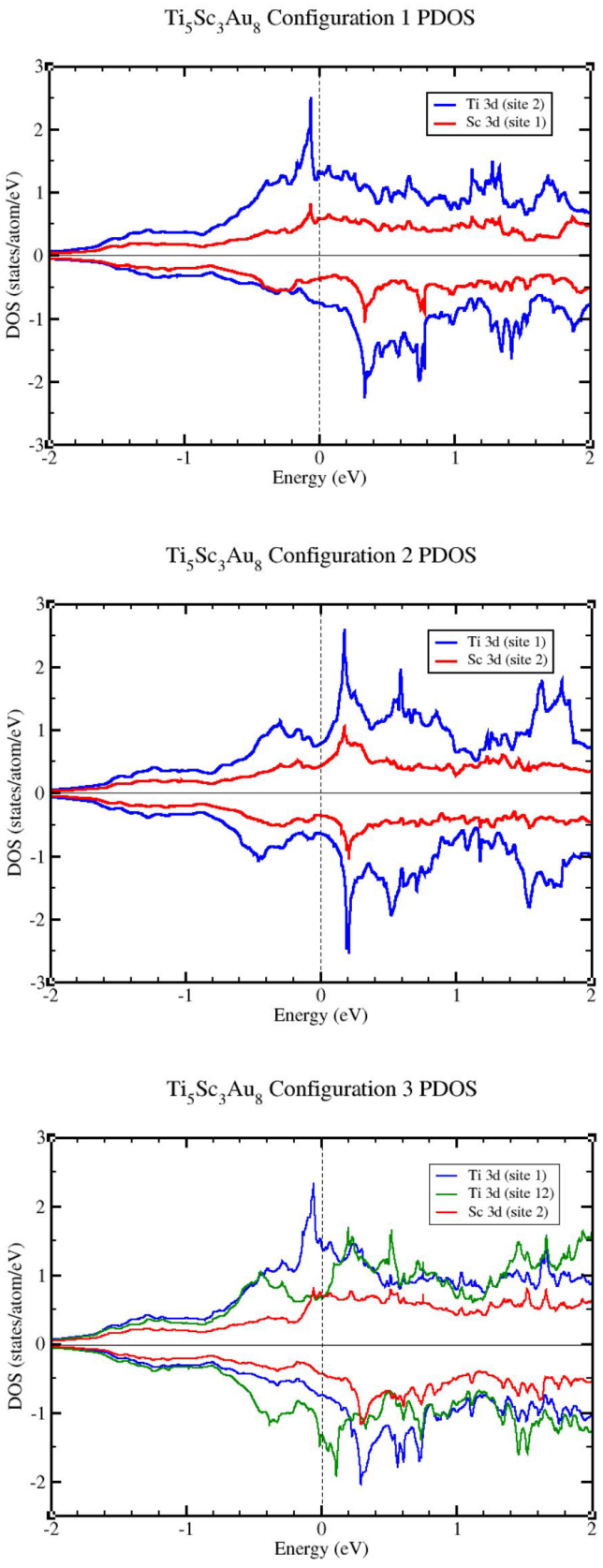

Figure 8. 3*d* projected DOS for $Ti_5Sc_3Au_8$ configurations C1, C2, C3. The PDOS shown in C2 are unpolarized: Sc(2) and one of the few dead Ti [Ti(1)] sites in our simulations; Ti(9) also has a quite weak polarization (table 3). Observe that this nonmagnetic Ti(1) site shows the same structure as does Sc(2) at 0.2 eV.

Table 3. Moments (μ_B) of the $Ti_5Sc_3Au_8$ for the three configurations C1, C2, C3. Site labels are in the first column, and Sc moments are in brackets.

Site	C1 moment	C2 moment	C3 moment
1	[−0.02]	[0.04]	0.59
2	0.58	[−0.05]	[0.06]
3	−0.38	−0.44	[0.08]
4	[0.07]	−0.50	[0.01]
9	0.75	0.13	0.25
10	0.26	[−0.05]	0.44
11	[0.09]	[−0.01]	−0.14
12	−0.21	−0.50	−0.14

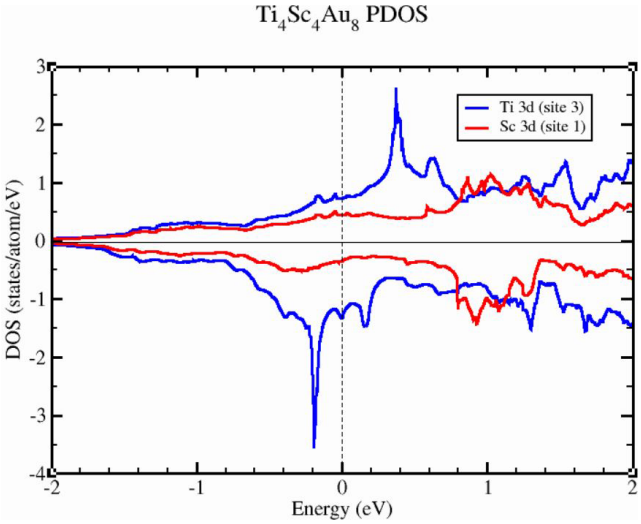

Figure 9. $x = 1/2$ $Ti_4Sc_4Au_8$ PDOS for the Sc-chain configuration discussed in the text with FM Ti chains. Note the vHs associated solely with the Ti states.

$a - b$ plane. The intact $\hat{b}$-axis directed chain has large *aligned* moments (TiAu itself has antialigned moments in this direction). C3 has two neighboring uninterrupted $\hat{b}$-axis Ti chains; the moments are aligned but their magnitudes are strongly affected by environment. One moment is 0.44 μ_B, the other is only 0.14 μ_B and might be considered to be induced by the neighboring Ti moments, rather than providing any real local moment.

The 3*d* PDOSs of selected sites for the three configurations are provided in figure 8. A general feature is that certain Ti sites persist in having a substantial peak in the PDOS centered around 0.2 eV below E_F. For the magnetic Ti sites (which is nearly but not quite all) this peak is spin split across E_F. With no splitting (C2) the peak lies *above* E_F. The peak lying below E_F for both spins would require more charge on that Ti site, at too much cost in Coulomb energy.

4.2.4. $x = 4/8$*:* $Ti_4Sc_4Au_8$. We performed one calculation with Ti $\hat{b}$-axis chains, either entirely Ti atoms or entirely Sc atoms, alternating along $\hat{c}$. The Ti chain, which is AFM ordered in TiAu, becomes *ferromagnetic* with large moments of 0.69 μ_B (50% larger than the bulk value in bulk TiAu), while the Sc chain is dead (small induced moments of 0.07 μ_B). Considering the separation of Ti layers perpendicular to the $\hat{c}$

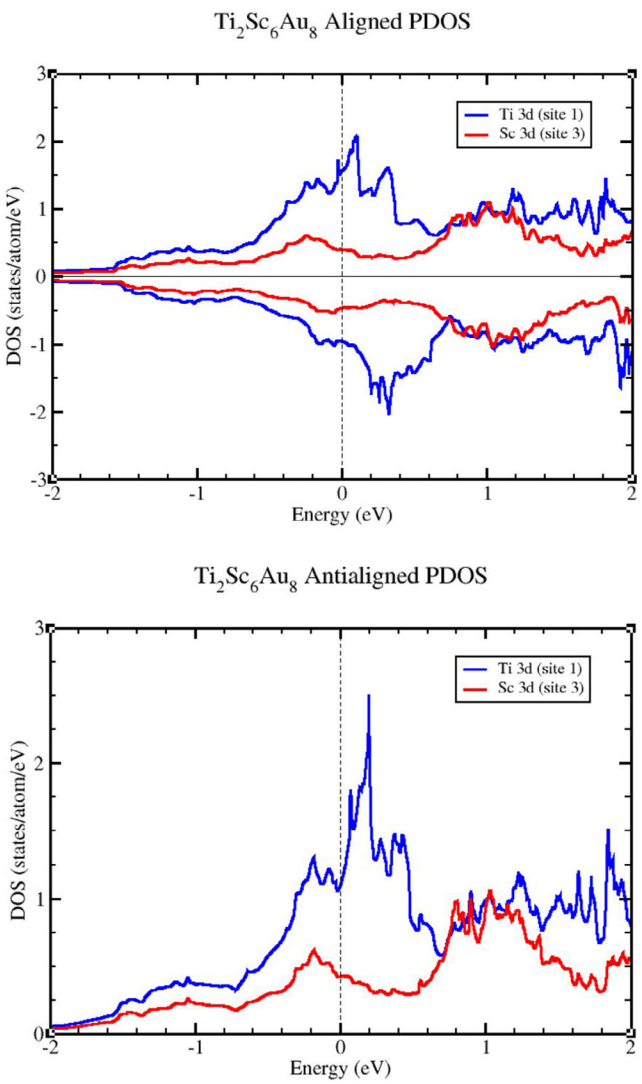

Figure 10. Top: the 3*d* PDOS for the aligned pair of Ti atoms $Ti_2Sc_6Au_8$. Again the Sc PDOS is unpolarized and structureless, with the peak arising solely from Ti *d* states. Bottom: the PDOS of the nonmagnetic state that resulted when initial Ti spins were antialigned.

axis, this configuration can be considered to be linear $\hat{b}$ axis chains, weakly coupled in the other two directions by RKKY interactions.

The PDOS of this supercell is shown in figure 9, showing similarities to other supercells. The FM exchange splitting across E_F is 0.6 eV, with the sharp vHs derived peaks having no contribution from Sc; Sc 3*d* character generally arises close to 1 eV above E_F.

4.2.5. $x = 6/8$*: $Ti_2Sc_6Au_8$.* In a pair of calculations, two near neighbor Ti atoms along the *b* direction were given aligned spins first, then given antialigned spins. When antialigned, the moments vanished giving a nonmagnetic state. When aligned, the Ti atoms each sustained a 0.36 μ_B moment. Just below, it is revealed that isolated Ti atoms are not magnetic within DFT. This result for $x = 6/8$ indicates the magnetic tendency is present already for the two-atom cluster, if the spins are

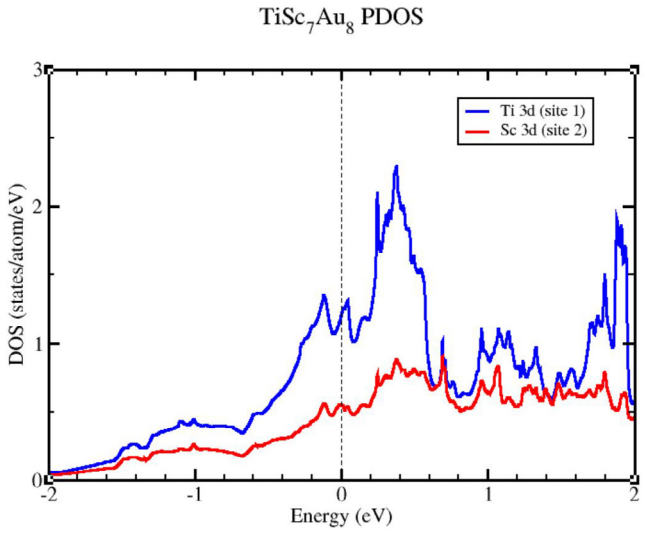

Figure 11. $x = 7/8$ $TiSc_7Au_8$ PDOS, comparing the Ti PDOS with that of one of the Sc sites. This single Ti atom case in nonmagnetic. Note also the lack of any sharp, narrow vHs peak.

aligned. Figure 10 presents the PDOS of the magnetic Ti and nonmagnetic Sc atoms, as well as the corresponding unpolarized PDOS that resulted when the calculation was begun with antialigned moments on Ti.

4.2.6. $x = 7/8$ *case: $TiSc_7Au_8$.* This brief focus was checking whether an (essentially) isolated Ti in (fictitious) ScAu would show a moment. The result was in the negative, the initially imposed moment vanishing during self-consistency. The resulting PDOS is provided in figure 11, where it can be seen that Ti provides strong peaks in $N(E)$ around and above E_F in the structureless background of the Sc 3*d* states.

4.2.7. Further comments about supercell studies. The FPLO code provides a separation of charge to specific atoms. The absolute values are not particularly meaningful. Variations with magnetism or amount of and geometric relation to Sc dopants could be revealing. Meaningful variations to not appear, however. The charges assigned to Ti or to Sc sites vary by only $\pm$ 0.01*e* from the mean, with the average for Ti sites being 1.01*e* greater than Sc. Thus charge transfer due to doping, and variation with amount of doping, are not factors in the effects of doping.

Surveying the results from the supercells, a few characteristics stand out.

1. Up to and somewhat beyond the concentration $x = \frac{1}{2}$, Ti atoms usually retain their moment. Sc never sustains a moment.
2. Two neighboring atoms in a layer with six Sc atoms are magnetic if spins are aligned; antialigned pairs of spins are energetically disfavored.
3. The underlying AFM ordering persists as Sc is added.
4. Ti moments do not decrease with increasing x, but retain values within $\pm$50% of the bulk value.
5. Ti 3*d* related peaks in the density of states persist in all of the ordered supercells.

5. Discussion and summary

The electronic and magnetic characteristics of $Ti_{1-x}Sc_xAu$ have been calculated from first principles methods for a number of doping fractions x from 1/8 to 7/8. The objective has been to determine whether the itinerant picture is appropriate for this alloy system, which is observed to undergo a QCP at $x_{cr} = \frac{1}{8}$. Previous indications have been that behavior follows an itinerant picture, in which case Moriya's theory of weak magnetism applies [29]. Taken literally, the picture would be that Ti moments decrease monotonically from their value at $x = 0$ to their zero values at $x = x_{cr}$. Fluctuations in the magnetism near the QCP can be characterized by their long wavelength components and the corresponding magnetic susceptibility. This picture of fluctuation is also prevalent, although less strictly applicable, in more strongly correlated materials where inhomogeneous behavior is evident from experimental data. These distinctions may be relevant for unusual behavior observed near the QCP in weak magnetics. In $Ti_{1-x}Sc_x$, non-Fermi liquid behavior is observed, as in several systems with clear strong local moment behavior.

Unlike the picture that has accounted for much of the behavior to the point, in our simulations we have found pervasive indications of Ti $3d$ local moment behavior in the Sc-substituted systems. Well beyond the QCP (up to $x = \frac{1}{2}$ and somewhat beyond), we find clear local Ti moment behavior. While the DFT methods we have used are known to overestimate magnetic tendencies in TiAu and similar systems, this tendency is confined to the itinerant regime, where only a mean Ti moment (considering our system) is involved. For the opposite limit of isolated (here, Ti) potential magnetic atoms in a non-magnetic matrix (ScAu), there is much less evidence to extrapolate from.

In the substituted supercells studied here, with just a few exceptions, Ti atoms remain magnetic well beyond the QCP concentration $x_{cr} = \frac{1}{8}$, with strong moments sometimes exceeding the bulk value. This indicates a strong tendency toward local moment behavior of Ti in $Ti_{1-x}Sc_xAu$. While a single Ti atom (or line of atoms along $\hat{c}$ in our calculation) is not magnetic, a pair of neighboring Ti atoms in the $\hat{s} - \hat{b}$ plane is magnetic with spins aligned. Without aligned spins, the moment vanishes. There is some competition between aligned and antialigned neighboring spins in this system.

Electron doping with vanadium $Ti_{1-y}V_yAu$ [17] was mentioned in the Introduction. A related system VAu_4, which is FM with an ordered moment of only 0.4 μ_B/V, has been studied theoretically by Khmelevska *et al* [30] using the coherent potential approximation method. Categorized as a wFM, the magnetic properties had been observed to depend strongly on the degree of chemical order. The calculations however indicated a definite local moment character of the V moment, seemingly similar to what we find for Ti in TiAu alloys. Another unusual result was that, using first principles methods that commonly predict the correct FM versus AFM order, AFM order was found to be favored over FM, in contradiction with observation.

Finally, we note the brief discussion in the Introduction of the special character of weak antiferromagnets near or somewhat beyond the QCP, where rare regions of AFM order coupled by long range RKKY interactions have been argued to promote a different type of magnetic ordering transition and related QCP than is the case for the simpler weak ferromagnet. We expect that further studies, both theoretical and experimental, on weak magnets should serve to clarify behavior near the quantum critical point.

Acknowledgments

The authors acknowledge helpful communication with E Svanidze and J M Santiago. This work was supported by NSF grant DMR-1607139.

ORCID iDs

Warren E Pickett https://orcid.org/0000-0003-4591-7691

References

[1] Matthias B T, Giorgi A L, Struebing V O and Smith J L 1978 Itinerant antiferromagnetism of $TiBe_2$ *Phys. Lett.* A **69** 221
[2] Enz C P 1981 On the possibility of weak itinerant antiferromagnetism in $TiBe_2$ *Physica* B + C **107** 77
[3] de Réotier P D, Lapertot G, Yaouanc A, Gubbens P C M, Sakarya S and Amato A 2006 Evidence for an antiferromagnetic component in the magnetic structure of $ZrZn_2$ *Phys. Lett.* A **349** 513
[4] Santiago J M, Huang C-L and Morosan E 2017 Itinerant magnetic metals *J. Phys.: Condens. Matter* **29** 373002
[5] Svanidze E *et al* 2015 An itinerant antiferromagnetic metal without magnetic constituents *Nat. Commun.* **6** 7701
[6] Pfleiderer C, Uhlarz M, Hayden S M, Vollmer R, Löhneysen H V, Bernhoeft N R and Lonzarich G G 2001 Coexistence of superconductivity and ferromagnetism in the d-band metal $ZrZn_2$ *Nature* **412** 58
[7] Kyker A B and Pickett W E 2005 Fermiology and Fulde–Farrell–Larkin–Ovchinnikov phase formation *Phys. Rev.* B **71** 224517
[8] Stoner E C 1938 Collective electron ferromagnetism *Proc. R. Soc.* A **165** 372
[9] Teacake S, Asoka H, Huang C Y and Smith J L 1981 No evidence of antiferromagnetism in $TiBe_2$—^{47}Ti and ^{49} Ti NMR *J. Phys. Soc. Japan* **50** 2137
[10] Jeong T, Kyker A and Pickett W E 2006 Fermi velocity spectrum and incipient magnetism in $TiBe_2$ *Phys. Rev.* B **73** 115106
[11] Hasegawa H and Moriya T 1974 Effect of spin fluctuations on itinerant electron antiferromagnetism *J. Phys. Soc. Japan* **36** 1542
[12] Moriya T and Ueda K 2003 Antiferromagnetic spin fluctuation and superconductivity *Rep. Prog. Phys.* **66** 1299
[13] Löhneysen H V, Rosch A, Vojta M and Wölfle P 2007 Fermi-liquid instabilities at magnetic quantum phase transitions *Rev. Mod. Phys.* **79** 1015
[14] Goh W F and Pickett W E 2016 A mechanism for weak itinerant antiferromagnetism: mirrored van Hove singularities *Europhys. Lett.* **116** 27004

[15] Goh W F and Pickett W E 2017 Competing magnetic instabilities in the weak itinerant antiferromagnetic TiAu *Phys. Rev.* B **95** 205124
[16] Svanidze E, Besara T, Wang J K, Geiger D, Prochaska L, Santiago J M, Lynn J W, Paschen S, Siegrist T and Morosan E 2017 Quantum critical point in the Sc-doped itinerant antiferromagnet TiAu *Phys. Rev.* B **95** 220405
[17] Huang C-L, Santiago J M, Svanidze E, Besara R, Siegrist T and Morosan E 2018 Effects of chemical disorder in the itinerant antiferromagnet $Ti_{1-x}V_xAu$ *J. Phys.: Condens. Matter* **30** 365602
[18] Narayanan R, Vojta T, Belitz D and Kirkpatrick T R 1999 Critical behavior of disordered quantum magnets: the relevance of rare regions *Phys. Rev.* B **60** 10150
[19] Dobrosavljevič V and Miranda E 2005 Absence of conventional quantum phase transitions in itinerant systems with disorder *Phys. Rev. Lett.* **94** 187203
[20] Vojta T 2006 Rare region effects at classical, quantum, and nonequilibrium phase transition *J. Phys. A: Math. Gen.* **39** R143–205
[21] Koepernik K and Eschrig H 1999 Full-potential nonorthogonal local-orbital minimum-basis band-structure scheme *Phys. Rev.* B **59** 1743
[22] Perdew J P and Wang Y 1992 Accurate and simple analytic representation of the electron-gas correlation energy *Phys. Rev.* B **45** 13244
[23] Perdew J P, Burke K and Ernzerhof M 1996 Generalized gradient approximation made simple *Phys. Rev. Lett.* **77** 3865
[24] Han M J, Yin Q, Pickett W E and Savrasov S Y 2009 Anisotropy, itineracy, and magnetic frustration in high T_c iron pnictides *Phys. Rev. Lett.* **102** 107003
[25] Sharma S, Shallcross S, Dewhurst J K, Sanna A, Bersier C, Massidda S and Gross E K U 2009 Magnetism in $CeFeAsO_{1-x}F_x$ and $LaFeAsO_{1-x}F_x$ from first principles *Phys. Rev.* B **80** 184502
[26] Ortenzi L, Mazin I I, Blaha P and Boeri L 2012 Accounting for spin fluctuations beyond local spin density approximation in the density functional theory *Phys. Rev.* B **86** 064437
[27] Sharma S, Gross E K U, Sanna A and Dewhurst J K 2018 Source-free exchange-correlation magnetic field in density functional theory *J. Chem. Theor. Comput.* **14** 1247
[28] Sigalas M M and Papaconstantopoulos D A 1994 Calculations of the total energy, electron–phonon interaction, and Stoner parameter for metals *Phys. Rev.* B **50** 7255
[29] Moriya T and Takahashi Y 1985 *Spin Fluctuations in Itinerant Electron Magnetism* (Berlin: Springer)
[30] Khmelevska T, Khmelevskyi S, Ruban A V and Mohn O 2007 Dependence of magnetism of VAu_4 alloy on the state of chemical order: a first principles study *Phys. Rev.* B **76** 054445